Extreme Mechanics Letters 37 (2020) 100699

Contents lists available at ScienceDirect

Extreme Mechanics Letters

journal homepage: www.elsevier.com/locate/eml

Atomistic simulations of the tensile behavior of graphene fibers

Lei Zhong [a], Huajian Gao [b,c,*], Xiaoyan Li [a,*]

[a] Center for Advanced Mechanics and Materials, Applied Mechanics Laboratory, Department of Engineering Mechanics, Tsinghua University, Beijing 100084, China
[b] School of Mechanical and Aerospace Engineering, College of Engineering, Nanyang Technological University, 70 Nanyang Drive, Singapore 639798, Singapore
[c] Institute of High Performance Computing, A*STAR, Singapore 138632, Singapore

ARTICLE INFO

Article history:
Received 28 January 2020
Received in revised form 14 March 2020
Accepted 17 March 2020
Available online 6 April 2020

Keywords:
Graphene fibers
Crack nucleation
Interlayer slipping
Structural continuity
Atomistic simulations
Graphene ruga sheets

ABSTRACT

In recent years, a large number of experimental studies have shown that graphene fibers, a new type of carbon fiber consisting of many monolayers of wrinkled and curved graphene sheets aligned in the axial direction of the fiber, exhibit high tensile strength and many functionalities. Although much effort has been devoted to improving their mechanical properties, the underlying deformation mechanism of graphene fibers under tension still remains unclear. Here, we construct simulation models of graphene fibers with diameters of 10 and 20 nm using wrinkled graphene sheets with topological defects, hereafter referred to as graphene ruga sheets, as building blocks via a combination of the phase field crystal method and atomistic modeling. We then perform a series of large-scale molecular dynamics simulations of the constructed graphene fibers under uniaxial tension. Our simulation results revealed that the graphene fibers undergo plastic deformation with stress flow and that their tensile strength (i.e., the peak stress in the stress–strain curve) and Young's modulus increase with decreasing fiber diameter, which is mainly attributed to the decrease in the number of defects with reduced fiber diameter. Our simulations further revealed that the tensile strength is related to nanocrack nucleation/initiation from nanovoids or sharp corners between neighboring fused graphene sheets, while the flow stress is determined by interlayer slipping between neighboring graphene layers. Furthermore, we investigated the influence of structural continuity on the tensile strength of graphene fiber. The results showed that the tensile strength increases 1.9-3.5 times with the improvement in the structural continuity of graphene fibers within the investigated range. Our simulations provide mechanistic insights into the deformation mechanism of graphene fibers, which may be used to guide their design and fabrication.

1. Introduction

Graphene fiber has emerged in recent years as a new type of carbon fiber with excellent mechanical properties and many functionalities. As a three-dimensional assembly of monolayer graphene, graphene fiber consists of many axially aligned, curved monolayer graphene sheets [1]. Due to its unique microstructure, graphene fiber exhibits superior mechanical, thermal and electrical properties, such as a high tensile strength and an excellent thermal and electrical conductivity [2–6], and thus has a wide range of potential applications in micro-/nanodevices, lightweight wires or cables, and wearable flexible devices [1]. Existing studies on graphene fibers have mainly focused on their fabrication, structural characterization and mechanical testing [1–9]. Macroscopic neat graphene oxide (GO) fibers and auspicated chemically reduced graphene fibers were first prepared by wet-spinning graphene liquid crystals [7]. These fibers are composed of a mass of curved GO or graphene sheets (with size around hundreds of nanometers) neatly arranged along the axial direction of the fiber. Tension tests showed that both GO and graphene fibers exhibit brittle fracture, with moduli of 5.4–7.7 GPa, tensile strengths of 100–140 MPa and fracture strains of 6%–7% [7]. Subsequently, stronger graphene fibers were successfully fabricated by wet-spinning giant GO liquid crystals, followed by wet-drawing and ion-cross-linking [9], achieving a modulus of 11.2 GPa, a tensile strength of 500 MPa, and fracture strain of ∼7% [9]. More optimized graphene fibers were recently fabricated by performing thermal annealing after wet-spinning [2]. Such optimized fibers contain both large (approximately 23 μm) and small (approximately 0.8 μm) reduced GO sheets [2], where large reduced GO sheets are neatly arranged along the axial direction of the fiber, while small reduced GO sheets randomly orient and fill in gaps among the large reduced GO sheets [2]. This

* Corresponding authors.
E-mail addresses: huajian.gao@ntu.edu.sg (H. Gao), xiaoyanlithu@tsinghua.edu.cn (X. Li).

https://doi.org/10.1016/j.eml.2020.100699
2352-4316/

unique microstructure enables the optimized graphene fiber to achieve modulus reaching 135 GPa, tensile strength up to 1.08 GPa, and fracture strain around 1.4% [2]. Furthermore, to improve the fracture resistance of graphene fiber, multiple reduced GO fibers can be twisted into a twisted hollow yarn that is stable. These twisted yarns have fracture energy of 43.6 J/m^3, which is 3–6 times higher than those of single reduced GO fibers [8], and tensile strength that can be controlled by adjusting the bias angle of individual constituent fibers [8].

So far, most existing studies [2–9] have mainly focused on the fabrication and characterization of microstructures and mechanical properties (including Young's modulus, tensile strength, and fracture strain or energy) of graphene fibers. However, the underlying deformation mechanisms that lead to these properties remain largely unclear. Moreover, the mechanical properties of graphene fibers are strongly influenced by the structural continuity of the constituent graphene sheets, and understanding how this occurs is of great interest.

In this paper, we first construct simulation samples of graphene fibers consisting of neatly arranged wrinkled graphene sheets with topological defects, referred to as graphene ruga sheets (GRSs), and then perform a series of large-scale molecular dynamics (MD) simulations of these graphene fibers under uniaxial tension. Our atomistic simulations not only show typical deformation features of graphene fibers under uniaxial tension but also reveal underlying deformation mechanisms. We further investigate the influence of structural continuity on the mechanical properties (especially tensile strength) of graphene fibers.

2. Methods

We construct atomic configurations of graphene fibers and then perform large-scale MD simulations for their uniaxial tension using the large-scale atomic/molecular massively parallel simulator (LAMMPS) [10]. The interatomic interactions are described by the adaptive intermolecular reactive empirical bond order (AIREBO) potential, which includes the bonded and nonbonded interactions (i.e., van der Waals interactions) between carbon atoms [11]. We use the software OVITO [12] to visualize the results of the MD simulations.

2.1. Construction of graphene fibers

According to typical microstructures of experimental samples, we first construct the full-atom configuration of graphene fibers. The graphene fibers used in experiments were composed of many curved graphene sheets neatly arranged along the axial direction of the fiber [1,9]. Scanning electron microscopy (SEM) images have shown that individual graphene sheets in graphene fibers have a wrinkled surface [9]. Based on the structural features of experimental samples, we constructed simulation samples with atomic structures similar to those of experimental samples [9] by using GRSs [13] as a building block, which are generated by using a combination of the phase field crystal (PFC) method and atomistic modeling [13]. The GRS structure is obtained by introducing selected topological defects in a graphene sheet, as shown in Fig. 1a. The PFC is first applied on a targeted ruga surface (top picture in Fig. 1a) to evolve a triangular pattern of continuum density waves to a minimum energy state (bottom picture in Fig. 1a). The obtained triangular pattern is then converted to a discrete triangular lattice by identifying the wave crests as nodes. Next, using Voronoi construction, the triangular lattice is transformed into a full-atom GRS structure, which is then equilibrated for 10 ps at a finite temperature via MD simulation. During equilibration, an isothermal–isobaric (NPT) ensemble is used to ensure a constant temperature of 300 K and zero pressure along the two in-plane directions of the graphene (Fig. 1b and c). Finally, a thermally stable GRS structure with in-plane dimensions (i.e., x_G-y_G in Fig. 1b) of 7 $\times$ 10 nm^2 is generated, as shown in Fig. 1b–d, where wrinkles are stabilized by the presence of disclination defects (e.g., pentagons and heptagons). The maximum amplitude of the wrinkle in the out-of-plane direction is up to 0.8 nm (i.e., z_G in Fig. 1b) due to the presence of the disclinations [14,15]. A larger GRS with dimensions of 7 $\times$ 20 nm^2 is generated by doubling the GRS in Fig. 1b along the y_G axis, where a few randomly distributed nanovoids with diameters of 1.4 nm are introduced by removing some atoms. In the GRSs we constructed, the topological defects mainly include the disclination defects, i.e. pentagons and heptagons. As shown in Fig. 1b and c, some pairs of pentagon and heptagon line up to form a grain boundary. It indicates that the GRSs we constructed are polycrystalline. The lengths of grain boundaries (i.e. chain of dislocations) are about 4–10 nm. If we define the number of disclination in per unit area as the defect density, the defect density of GRS we constructed is about 0.86 nm^{-2}.

Fig. 1e shows a schematic illustration of the construction process of graphene fibers using tens of GRS structures. First, some GRSs are placed in a simulation box with dimensions of 20 $\times$ 20 $\times$ 20 nm^3. The length direction of GRS is aligned in parallel to the z axis of the simulation box, and its normal direction is randomly oriented in the x-y plane of the box, as illustrated by Fig. 1e. The entire system is then equilibrated via dynamic relaxation at 300 K for 50 ps under an NPT ensemble. During equilibration, periodic boundary condition is imposed in the z axis. After equilibration, the simulation system is squeezed by shrinking a constraining cylindrical surface that surrounds the system and is parallel to the z axis. The strain rate of squeezing is up to 10^9 s^{-1}. During squeezing, a canonical (NVT) ensemble is used to ensure a constant temperature of 300 K. The squeezing is terminated when the in-plane diameter of the simulated system reaches 10 nm. After squeezing, a melting-and-quenching process is applied to the simulation system. Throughout this process, the volume of the simulated system is kept constant by fixing both the diameter of the cylindrical confinement and the dimension of the simulation box in the z axis. During this process, the temperature is first increased from 300 K to 1200 K within 50 ps, then kept at 1200 K for 200 ps, and finally decreased to 300 K within 50 ps. This process is used to accelerate the fusion of defective graphene sheets, which involves the formation of new sp^2 or sp^3 bonds between atoms with dangling bonds on the edges of GRSs or nanovoids. Notably, the fusion location between neighboring GRSs can act as the sites for crack nucleation due to the stress concentration, as indicated by the subsequent simulations of uniaxial tension of graphene fibers. After the melting-and-quenching process, the cylindrical confinement is removed, and the simulation system is relaxed at 300 K for 200 ps under an NPT ensemble to ensure zero pressure along the z axis. The right picture in Fig. 1f shows the atomic configuration of a typical constructed graphene fiber with a diameter (D) of 10 nm and length (L) of 20 nm. The density of this graphene fiber is approximately 1.36 g cm^{-3}, which is close to those (approximately 1.0–1.4 g cm^{-3}) of experimental samples [1,2]. In the constructed graphene fibers, the typical spacings between adjacent graphene layers are about 0.34 nm, which is close to the equilibrium interlayer spacing given by the Van der Waals interaction function used in the AIREBO potential. Previous experimental observations [2–8] have shown that the graphene sheets of experimental graphene fibers are significantly winkled, which is an important microstructural feature associated with mechanical properties of graphene fibers. Such wrinkling is generated due to presence of complicated topological defects (especially disclination defects). To mimic such wrinkled feature of

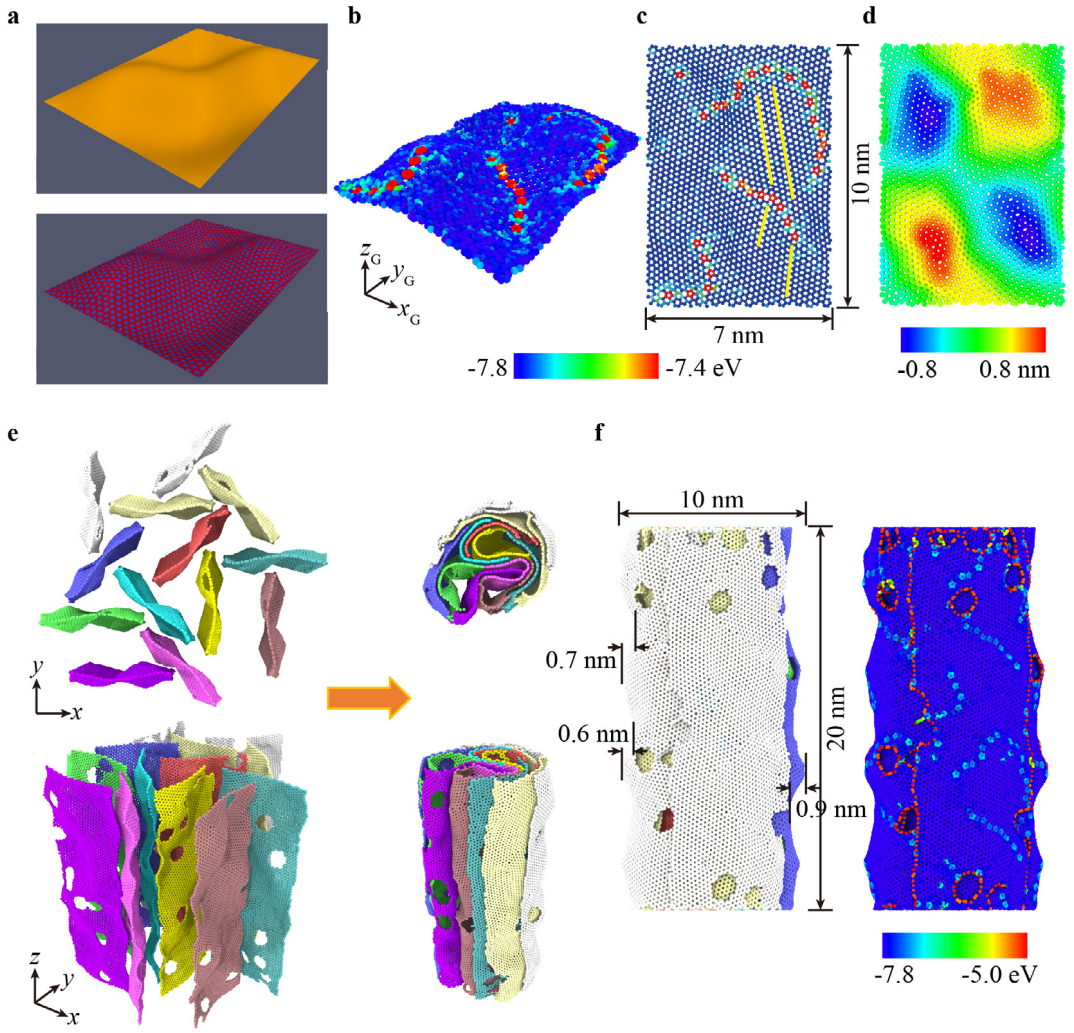

Fig. 1. (a) Geometric model of a ruga surface (top) and a continuous triangular pattern of density waves on the ruga (bottom). (b,c,d) Atomic configurations of typical GRS in different views. The colors in (b,c) and (d) represent the potential energy and out-of-plane coordinates (i.e., along the z_G direction) of the atom, respectively. The yellow lines are used to indicate the misorientation between neighboring grains. (e) Schematic illustration of the construction process of a graphene fiber consisting of GRSs. (f) Atomic configurations of typical constructed graphene fibers. The colors in the left and right pictures represent the layer number of the constituent GRS and the potential energy of the atom. (For interpretation of the references to color in this figure legend, the reader is referred to the web version of this article.)

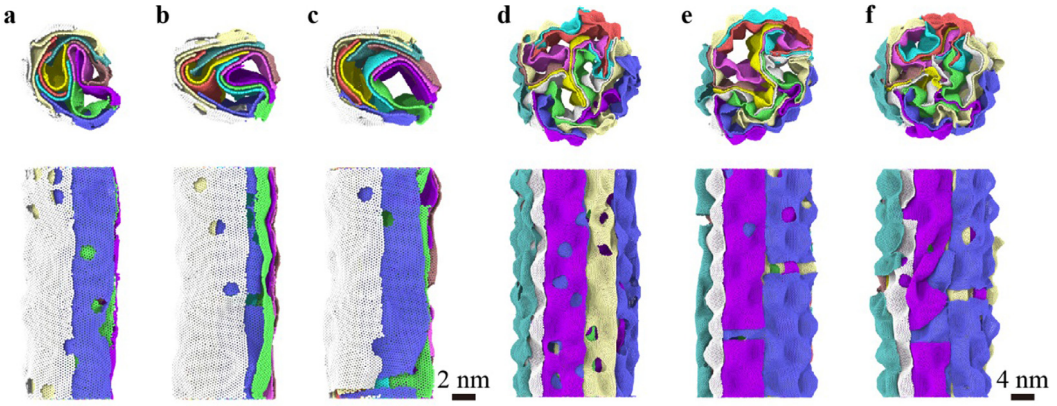

Fig. 2. (a–c) Top and front views of the atomic configurations of three graphene fibers with $D = 10$ nm and $F_{sG} = 1$, ~0.5 and 0, respectively. (d–e) Top and front views of the atomic configurations of three graphene fibers with $D = 20$ nm and $F_{sG} = 1$, 0.5 and 0, respectively.

experimental samples, we used the GRSs with disclination defects instead of flat graphene sheets without ruga structures to construct the simulated samples. The disclination defects can induce the wrinkling of graphene sheets and reduce their moduli [14,15]. During construction, the density and distribution of disclination defects are controlled to adjust the amplitude of wrinkles. Fig. 1f

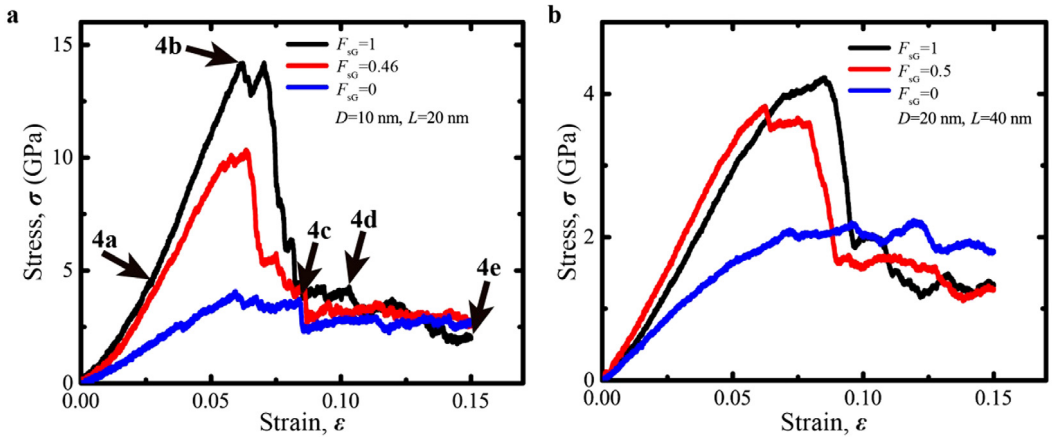

Fig. 3. (a,b) Uniaxial tensile stress–strain curves of graphene fibers with $D = 10$ nm and $D = 20$ nm, respectively.

shows that the constructed graphene fiber has a wrinkled surface with an asperity amplitude of 0.6–0.9 nm. The ratio of the fiber diameter to wrinkle amplitude of the constructed samples is close to those of experimental samples [9].

In the constructed graphene fibers, all the constituent GRSs are continuous along the z axis (i.e., tensile direction in subsequent tension simulations). The mechanical properties of a graphene fiber are determined by its structural continuity (i.e., the continuity of individual constituent graphene sheets along the tensile direction). In our simulations, we can control the structural continuity of a constructed graphene fiber by severing some constituent GRSs in the fiber. The severing is achieved by randomly removing a small strip of atoms in the horizontal plane of a selected GRS (i.e., x-y plane). Here, we define F_{sG} as the fraction of nonsevered GRSs in a graphene fiber to characterize its structural continuity. For example, for a graphene fiber containing 13 GRSs (which are continuous along the z axis), if 0, 7 and 13 GRSs are severed, then $F_{sG} = 1$, ∼0.5 and 0, respectively. The top and front views of three graphene fibers with $F_{sG} = 1$, ∼0.5, and 0 are shown in Fig. 2a, b and c, respectively. Fig. 2d, e and f show the atomic configurations of graphene fibers with $D = 20$ nm and $F_{sG} = 1$, 0.5 and 0, respectively. These graphene fibers consist of 22 GRSs with dimensions of 14×40 nm^2 and wrinkling amplitude of 1.6 nm. The diameter of voids introduced in these GRSs is up to 2.8 nm. As a result, the density of the graphene fibers with $D = 20$ nm is approximately 1.0 g cm^{-3}. It is noted that introduction of nanovoids in simulated graphene fiber is used to mimic the real experimental samples which contain some voids of size of 3–5 μm due to the chemical and physical processing during fabrication [4]. The size of nanovoids is set as 1.4 and 2.8 nm for simulated fibers with diameters of 10 and 20 nm, respectively, in order to ensure the density of simulated samples to be close to that of experimental samples.

2.2. Simulations on uniaxial tension

We perform a series of MD simulations on uniaxial tension of all the constructed graphene fibers with $D = 10$ and 20 nm. During the simulations, the graphene fibers are stretched along the axial direction of the fiber at a constant strain rate of 5×10^8 s^{-1} under an NVT ensemble. The temperature is kept at a constant 300 K, and the periodic boundary condition is imposed in the axial direction of the fiber. During the simulations, the stress components of each atom are calculated via the Virial theorem. The tensile stress of the entire fiber is obtained by averaging the axial stresses of all the atoms.

3. Results and discussion

3.1. Stress–strain curves and mechanical properties

Fig. 3a–b present the uniaxial tensile stress–strain curves from MD simulations for graphene fibers with $D = 10$ and 20 nm, respectively. The results show that all the simulated fibers first undergo a linear elastic deformation. After the elastic deformation, the stress fluctuates slightly as the applied strain increases. After the stress reaches a peak, it suddenly drops to a lower level and then exhibits a flow trend. These deformation features indicate that the simulated graphene fibers can undergo plastic deformation, which is different from previous experimental observations [1,2,9] where the graphene fibers fail via brittle fracturing after elastic deformation. The reason for this difference may be that the experimental samples have more defects or flaws, so more microcracks can initiate from these defects or flaws and then rapidly propagate after the elastic stage, leading to brittle fracture of the entire fiber. We further explain such differences in deformation features between the simulated and experimental samples when discussing the deformation mechanisms in the next section.

By fitting the slope of the linear elastic regime in the stress–strain curve, we obtained the Young's modulus of the graphene fiber. We used the peak stress in the stress–strain curve as the tensile strength of the graphene fiber. Table 1 summarizes the moduli and tensile strengths of simulated samples with different diameters and F_{sG} values. The modulus of the simulated fiber varies from 37 to 285 GPa, which is much higher than that (5.4–11.2 GPa) of most recently studied experimental fibers [1,7,9] but comparable to that (∼135 GPa) of optimized experimental fibers [2]. The tensile strength of the simulated fiber ranges from 2.1 to 14 GPa, which is higher than that (0.5–1.08 GPa) of experimental fibers. The higher moduli and strengths of the simulated samples imply that the simulated fibers are more ideal and have fewer defects and flaws than the experimental samples. The higher strengths of the simulated samples are also partly related to the ultrahigh strain rate used in the MD simulations, which is several orders of magnitude higher than that used in experiments. It is seen from Table 1 that for a given diameter, as the structural continuity decreases (i.e., F_{sG} decreases), both the modulus and strength of the simulated fiber decrease significantly. This is easily explained by the fact that with the reduction in structural continuity, the number of continuous GRSs that can bear applied loading in the fiber decreases. It is noted that for the simulated samples with $D = 20$ nm, the Young's modulus of sample with $F_{sG} = 0.5$ is slightly higher than that of sample with

Table 1
Young's moduli and tensile strengths of the simulated fibers with different diameters and F_{sG} values.

F_{sG}	Young's modulus (GPa)		Tensile strength (GPa)	
	$D = 10$ nm	$D = 20$ nm	$D = 10$ nm	$D = 20$ nm
1	285	62	14.0	4.2
0.5	200	70	10.2	3.8
0	74	37	4.0	2.1

$F_{sG} = 1$. The reason is that the density (1.01 g cm^{-3}) of sample with $D = 20$ nm and $F_{sG} = 0.5$ is just slightly larger than that (0.90 g cm^{-3}) of sample with $D = 20$ nm and $F_{sG} = 1$.

3.2. Deformation mechanisms

Fig. 4a–e capture a sequence of snapshots of stretched graphene fibers with $D = 10$ nm and $F_{sG} = 1$ at different tensile strains which are labeled in Fig. 3a. In the initial elastic stage, the wrinkled GRSs become flat due to stretching (Fig. 4a). As the applied tensile strain increases, multiple nanoscale cracks initiate/nucleate from the edges of preexisting nanovoids due to stress concentration and rapidly propagate along a direction perpendicular to the stretch direction, leading to abrupt fracturing of the GRSs (Fig. 4b and c). Such failure events give rise to a large stress drop at a tensile strain of approximately 6.2%, as evidenced by Fig. 3a. A similar phenomenon is observed in all the simulated fibers. It is noted that when the nanocracks nucleate, the stress simultaneously reaches its peak value along the stress–strain curve. Therefore, the peak stress (i.e., tensile strength mentioned above) signals crack initiation/nucleation. In all our MD simulations, the strains for crack initiation/nucleation are in the range from ∼5% to 9%, which are close to the fracture strains (∼1.4%–7%) of experimental samples [2,9]. After some constituent GRSs fracture, interlayer slipping/shear occurs between neighboring GRSs (Fig. 4d and e). Although the interaction between neighboring GRSs is relatively weak, interlayer slipping/shear becomes the main mechanism for bearing the applied loading of graphene fiber after most of the GRSs fracture. As a result, the stress does not drop to zero but fluctuates along a plateau, exhibiting a stress flow, as shown in Fig. 3a and b. This indicates that the simulated fibers can undergo a certain plastic deformation due to interlayer slipping/shear, which is distinct from the typical brittle fracture of experimental fibers after elastic deformation [1,2,9]. At the stress flow stage, a few nanocracks propagate by coalescing with some defects (such as vacancies, disclinations and dislocations) ahead of the crack tip (Fig. 4e). For the simulated fiber with $D = 20$ nm, nanocracks also nucleate from the edge of the nanovoids. However, during propagation, these cracks interact with some distributed dislocations, leading to the formation of single-atom chains along the crack propagation paths, indicating crack bridging at the atomic scale. This phenomenon has also been reported in previous MD simulations of crack propagation in individual GRSs [13]. This atomic-scale crack bridging is attributed to the influence of the uniform stress field induced by the distributed dislocations on the crack propagation [13]. Such a mechanism can contribute to the stress flow and the enhanced fracture energy of graphene fibers.

Fig. 5a and b show snapshots of stretched graphene fibers with $D = 10$ nm and $F_{sG} = 0$ (meaning that all constituent GRSs are discontinuous and severed) at 5.9% and 8.6% strain, respectively. During sample construction, the discontinuous GRSs might fuse with neighboring GRSs during the melting-and-annealing process, leading to the formation of sharp corners (Fig. 5a), where nanocracks can nucleate during stretching. A similar phenomenon is seen during extension of the fiber with $D = 20$ nm

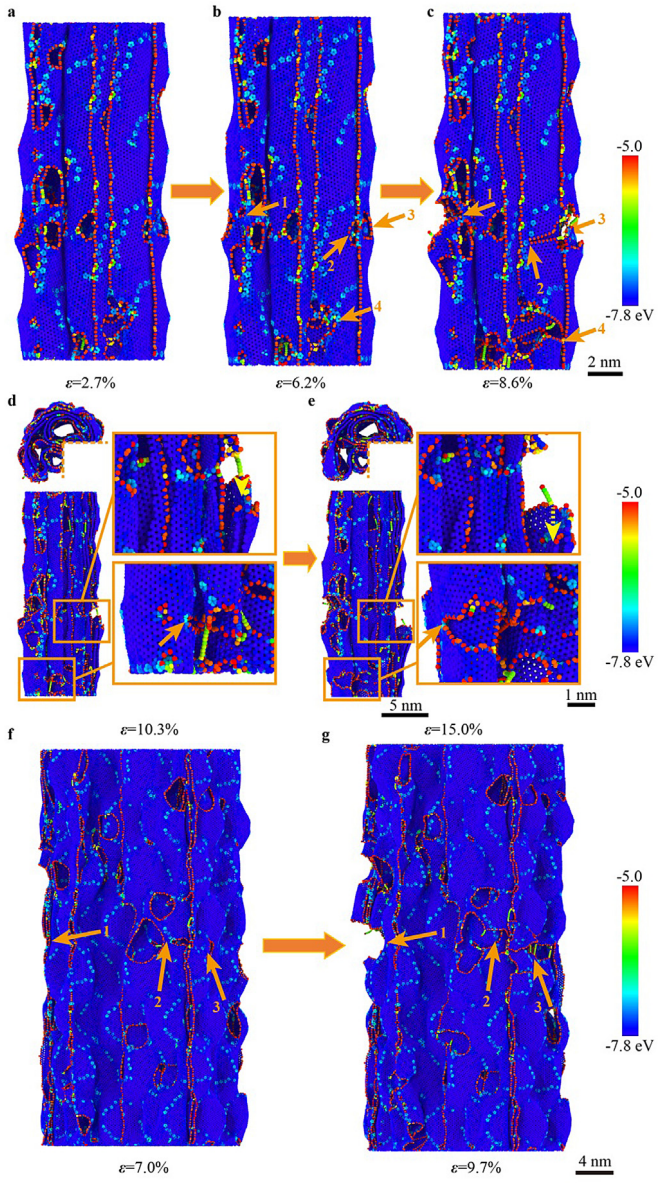

Fig. 4. (a–c) A sequence of snapshots of stretched graphene fiber with $D = 10$ nm and $F_{sG} = 1$ at different strains. The nanocracks nucleate from the stress concentration sites around nanovoids and then rapidly propagate, as indicated by arrows labeled by numbers. (d–e) Snapshots of stretched graphene fiber with $D = 10$ nm and $F_{sG} = 1$ at 10.3% and 15.0% strain, respectively, indicating interlayer slipping/shear between neighboring GRSs at the stress flow stage. The yellow arrows indicate the slipping direction of the GRSs. (f–g) Snapshots of stretched graphene fiber with $D = 20$ nm and $F_{sG} = 1$ at 7.0% and 9.7% tensile strain, indicating crack nucleation and atomic bridging during crack propagation. The colors in all these figures represent the potential energy of the atom. (For interpretation of the references to color in this figure legend, the reader is referred to the web version of this article.)

and $F_{sG} = 0$, as evidenced by Fig. 5c and d. It is noted that in the fibers with $F_{sG} = 0$, all the constituent GRSs are discontinuous and severed. In this case, the interlayer slipping/shear between neighboring GRSs dominates the plastic deformation of the graphene fiber. As a result, there is no apparent stress drop in the stress–strain curves, and the peak stress is close to the flow stress (i.e. the stress level at the flow stage), as shown in Fig. 3a and b.

Our MD simulations showed that the tensile strength of graphene fiber is related to nanocrack nucleation/initiation in

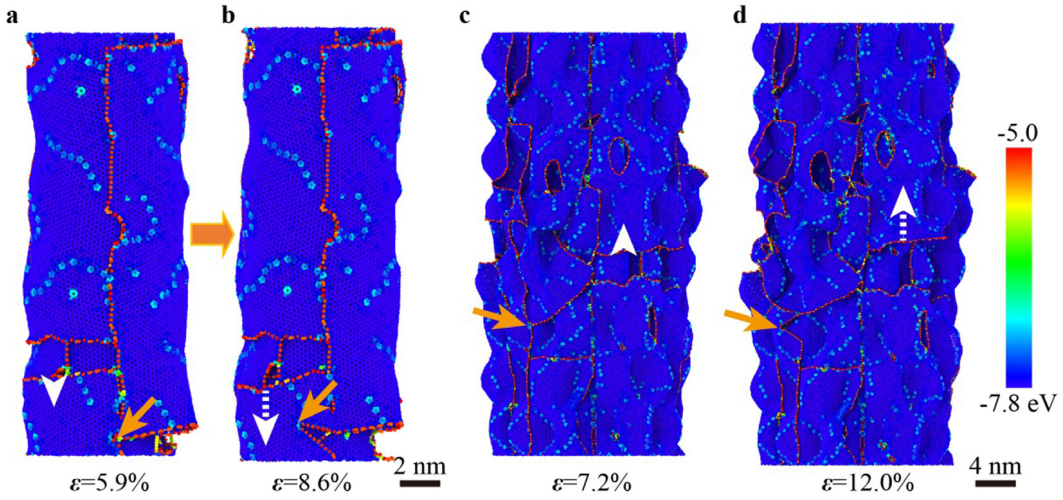

Fig. 5. (a,b) Snapshots of stretched graphene fiber with $D = 10$ nm and $F_{sG} = 0$ at 5.9% and 8.6% strain, respectively. (c,d) Snapshots of stretched graphene fiber with $D = 20$ nm and $F_{sG} = 0$ at 7.2% and 12.0% strain, respectively. These pictures indicate crack nucleation from the fusion location between neighboring GRSs and interlayer slipping/shear. The white arrows indicate the slipping direction of the GRSs. The colors in all these figures represent the potential energy of the atom. (For interpretation of the references to color in this figure legend, the reader is referred to the web version of this article.)

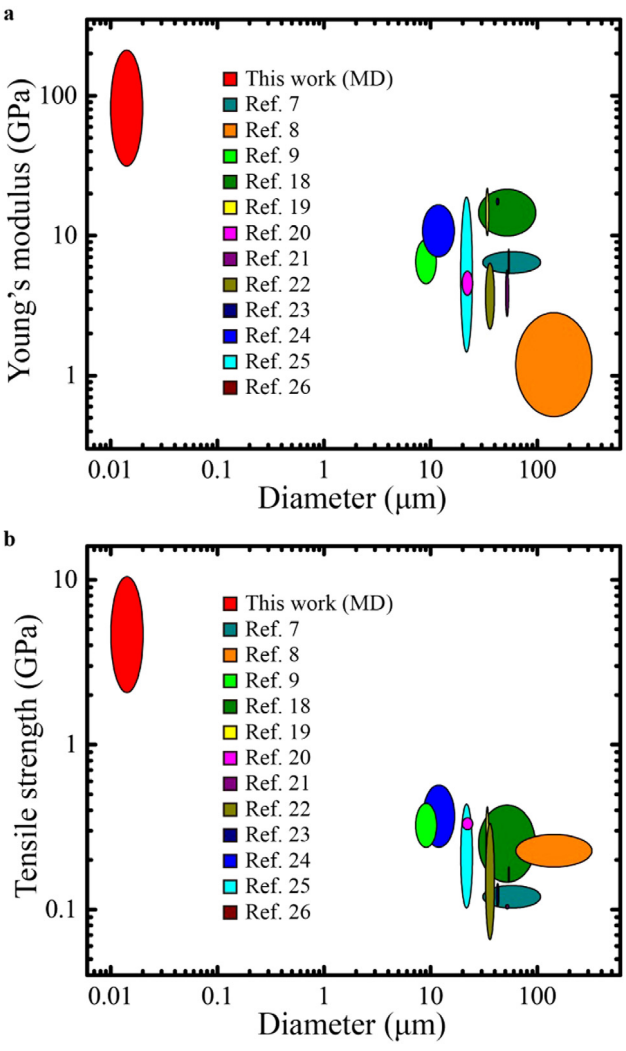

Fig. 6. (a,b) Young's modulus and tensile strength versus graphene fiber diameter. Data from our simulations and previous experiments [7,8,16–24] are included. As the diameter of the graphene fiber decreases, both the Young's modulus and tensile strength increase significantly.

the constituent GRSs. Notably, the nanocracks mainly nucleate/initiate from the edges of the nanovoids or the sharp corners of neighboring fused GRSs. Therefore, if the nanovoids and sharp corners related flaws can be reduced in the experimental fibers, then the tensile strength of the fiber can be enhanced significantly. Furthermore, in our simulated samples, the interaction between neighboring constituent GRSs is mainly via the van der Waals force, which contributes to a high stress level of approximately 2 GPa at the flow stage. As the van der Waals interaction is much weaker than covalent bonding, it can be speculated that similar to other 3D assemblies of graphene (such as carbon fibers [25] and pyrolytic carbon micropillars [26]), introducing strong covalent cross-links or bonds between neighboring constituent GRSs could significantly improve the tensile strength of graphene fibers.

3.3. Size dependences of Young's modulus and tensile strength

Fig. 6a and b present the variations in Young's modulus and tensile strength of graphene fibers with the fiber diameter, respectively. The data included in Fig. 6a–b are from our MD simulations and previous experiments [7,8,16–24]. In the experimental data, both the Young's modulus and tensile strength generally increase with decreasing diameter. Our simulations also show the same trend, i.e., the fiber with $D = 10$ nm has a higher Young's modulus and tensile strength than the one with $D = 20$ nm (see Table 1). Such size dependences can be attributed to the concentration and size of defects or flaws in the simulated fibers. It is easily understood that larger samples with more defects or flaws facilitate crack nucleation and hence have lower tensile strength. At the same time, the presence of more defects or flaws results in a decrease in Young's modulus. Therefore, the reduction in defect size and concentration contributes to enhanced Young's modulus and tensile strength. Furthermore, it is noted that the simulated fiber with $D = 10$ nm is more compact and has a higher density than the one with $D = 20$ nm. This suggests that improving the compactness and density of graphene fibers may facilitate further improvement in their tensile strength.

4. Conclusions

In summary, we constructed full-atom graphene fibers with microstructures similar to those of experimental samples by using GRSs as building blocks. These constructed fibers consist of

wrinkled and curved GRSs neatly arranged parallel to the axial direction of the fiber. We further performed a series of large-scale MD simulations of the constructed fibers under uniaxial tension. Our simulation results revealed that during stretching, the nanocracks nucleate/initiate from the nanovoids or sharp corners between neighboring fused GRSs, which determines the tensile strength of the graphene fiber. At the stress flow stage, interlayer slipping/shear becomes a dominant deformation mechanism. Our simulations also showed that the Young's modulus and tensile strength of graphene fiber are significantly dependent on the structural continuity and defect size and concentration. Our study not only sheds light on the fundamental deformation mechanisms of graphene fibers but may also provide guidance for the design and synthesis of high-performance graphene fibers.

Declaration of competing interest

The authors declare that they have no known competing financial interests or personal relationships that could have appeared to influence the work reported in this paper.

Acknowledgments

X.L. gratefully acknowledges the financial support from the National Natural Science Foundation of China (Grant Nos. 11522218, 91963117 and 11720101002). H.G. acknowledges financial support from the National Science Foundation (Grant No. DMR-1709318). All the simulations were performed on the TianHe-1 supercomputer at the National Supercomputer Center in Tianjin.

References

[1] Z. Xu, C. Gao, Graphene fiber: a new trend in carbon fibers, Mater. Today 18 (2015) 480–492.
[2] G. Xin, et al., Highly thermally conductive and mechanically strong graphene fibers, Science 349 (2015) 1083–1087.
[3] G. Qu, et al., A fiber supercapacitor with high energy density based on hollow graphene/conducting polymer fiber electrode, Adv. Mater. 28 (2016) 3646–3652.
[4] J. Yu, et al., Ultrahigh-rate wire-shaped supercapacitor based on graphene fiber, Carbon 119 (2017) 332–338.
[5] J. Zhang, et al., δ-MnO_2/holey graphene hybrid fiber for all-solid-state supercapacitor, J. Mater. Chem. A 4 (2016) 9088–9096.
[6] B. Zheng, et al., Graphene fiber-based asymmetric micro-supercapacitors, J. Mater. Chem. A 2 (2014) 9736–9743.
[7] Z. Xu, C. Gao, Graphene chiral liquid crystals and macroscopic assembled fibers, Nature Commun. 2 (2011) 571.
[8] X. Xiang, et al., In situ twisting for stabilizing and toughening conductive graphene yarns, Nanoscale 9 (2017) 11523–11529.
[9] Z. Xu, et al., Ultrastrong fibers assembled from giant graphene oxide sheets, Adv. Mater. 25 (2013) 188–193.
[10] S. Plimpton, Fast parallel algorithms for short-range molecular dynamics, J. Comput. Phys. 117 (1995) 1–19.
[11] S.J. Stuart, A.B. Tutein, J.A. Harrison, A reactive potential for hydrocarbons with intermolecular interactions, J. Chem. Phys. 112 (2000) 6472–6486.
[12] A. Stukowski, Visualization and analysis of atomistic simulation data with OVITO-the Open Visualization Tool, Model. Simul. Mater. Sci. 18 (2009) 015012.
[13] T. Zhang, X. Li, H. Gao, Designing graphene structures with controlled distributions of topological defects: A case study of toughness enhancement in graphene ruga, Extreme Mech. Lett. 1 (2014) 3–8.
[14] Y. Wei, et al., The nature of strength enhancement and weakening by pentagon–heptagon defects in graphene, Nature Mater. 11 (2012) 759–763.
[15] A. Fox, U. Ray, T. Li, Strength of graphene grain boundaries under arbitrary in-plane tension, Carbon 142 (2019) 388–400.
[16] R. Jalili, et al., Scalable one-step wet-spinning of graphene fibers and yarns from liquid crystalline dispersions of graphene oxide: towards multifunctional textiles, Adv. Funct. Mater. 23 (2013) 5345–5354.
[17] Z. Dong, et al., Facile fabrication of light, flexible and multifunctional graphene fibers, Adv. Mater. 24 (2012) 1856–1861.
[18] Z. Xu, et al., Highly electrically conductive ag-doped graphene fibers as stretchable conductors, Adv. Mater. 25 (2013) 3249–3253.
[19] H. Cheng, et al., Moisture-activated torsional graphene-fiber motor, Adv. Mater. 26 (2014) 2909–2913.
[20] Z. Liu, et al., Lyotropic liquid crystal of polyacrylonitrile-grafted graphene oxide and its assembled continuous strong nacre-mimetic fibers, Macromolecules 46 (2013) 6931–6941.
[21] Y. Hu, et al., All-in-one graphene fiber supercapacitor, Nanoscale 6 (2014) 6448–6451.
[22] X. Hu, et al., Liquid crystal self-templating approach to ultrastrong and tough biomimic composites, Sci. Rep. 3 (2013) 2374.
[23] X. Zhao, et al., Macroscopic assembled, ultrastrong and H_2SO_4-resistant fibres of polymer-grafted graphene oxide, Sci. Rep. 3 (2013) 3164.
[24] H.P. Cong, et al., Wet-spinning assembly of continuous, neat, and macroscopic graphene fibers, Sci. Rep. 2 (2012) 613.
[25] X. Qin, et al., A comparison of the effect of graphitization on microstructures and properties of polyacrylonitrile and mesophase pitch-based carbon fibers, Carbon 50 (2012) 4459–4469.
[26] X. Zhang, et al., Theoretical strength and rubber-like behaviour in micro-sized pyrolytic carbon, Nature Nanotechnol. 14 (2019) 762–769.